Heat-release equation of state and thermal conductivity of warm dense carbon by proton differential heating

Yuan Ping,[1,*] Heather D. Whitley,[1] Andrew McKelvey,[1,2] Gregory E. Kemp,[1] Phillp A. Sterne,[1] Ronnie Shepherd,[1] Marty Marinak,[1] Rui Hua,[3] Farhat N. Beg,[3] and Jon H. Eggert[1]

[1]*Lawrence Livermore National Laboratory, Livermore, California 94550, USA*

[2]*University of Michigan, Ann Arbor, Michigan 48109, USA*

[3]*University of California San Diego, La Jolla, California 92093, USA*

(Received 20 August 2018; revised manuscript received 18 July 2019; published 17 October 2019)

Warm dense carbon is generated at 0.3–2.0 g/cc and 1–7 eV by proton heating. The release equation of state (EOS) after heating and thermal conductivity of warm dense carbon are studied experimentally in this regime using a Au/C dual-layer target to initiate a temperature gradient and two picosecond time-resolved diagnostics to probe the surface expansion and heat flow. Comparison between the data and simulations using various EOSs and thermal conductivity models is quantified with a statistical χ^2 analysis. Out of seven EOS tables and five thermal conductivity models, only L9061 with the Lee-More model provides a probability above 50% to match all data.

DOI: 10.1103/PhysRevE.100.043204

I. INTRODUCTION

Carbon, in various natural structures, is an important material with wide applications in many research areas. For studies in the field of high-energy-density physics [1], it is employed as an ablator in inertial confinement fusion (ICF) targets [2] and serves as a high-strength tamping material in compression experiments [3,4], and its properties under extreme pressures are essential for planetary sciences [5,6]. In the warm dense matter (WDM) regime where the temperature is comparable to Fermi temperature and the kinetic energy is comparable to interparticle potential energy, the equation-of-state (EOS) and thermophysical properties of carbon are critical for modeling of planet formation and developing predictive capability of ICF performance.

Despite both theoretical and experimental challenges in the WDM regime, progress has been made to advance the understanding of WDM properties. On the modeling side, average-atom models [7–9], molecular dynamics simulations [10–12], and density function theory calculations [13–16] have been developed to calculate EOSs and conductivities. On the experimental side, measurements of carbon properties under extreme conditions have been enabled by recent development of laser-driven platforms in various facilities, such as melting temperature along Hugoniot [6], EOSs along low-temperature isentropes by ramp compression [17,18], and strong shock-release EOSs [19,20]. However, the high-temperature, off-Hugoniot warm dense region is still a largely uncharted area. This region is of importance for preheat characterization in ICF targets [21], hot electron transport in fast ignition [22], as well as applications such as laser micro-machining, etc. A heating experiment can fill such a gap in the carbon phase diagram.

In this paper we present an experimental study of heat-release EOSs and thermal conductivity (κ_t) of amorphous carbon in a density range of 0.3–2.0 g/cc (g/cm^3) and a temperature range of 1–7 eV. The experiment was performed using the proton differential heating platform [23], which has provided measurements on Au and Al [24]. The design concept is quite simple [23]: a temperature gradient is initiated between Au and C by different energy deposition in these two materials; the subsequent heat flow from the hotter Au to the cooler C rear surface is detected with two time-resolved optical diagnostics with ps-time resolution. Comparison between the data and simulations using various EOS and κ_t models is quantified with a statistical χ^2 analysis to determine probabilities of each model to match the data. It is found that the L9061 EOS table together with $1.05 \pm 0.15\times$ Lee-More thermal conductivity model provides the best agreement with the data within the experimental errors. Potential improvements for future experiments are also discussed.

II. EXPERIMENTAL SETUP

The experiment was performed on the Titan laser at the Jupiter laser facility (JLF) at Lawrence Livermore National Laboratory (LLNL). The setup is shown in Fig. 1(a). Details of the setup have been described in our previous paper on Al [24]. MeV protons generated by high-intensity laser-foil interaction were used as the heating source, a standard approach for volumetric heating to reach WDM states [25–27]. The proton energy spectrum was recorded every shot by a Thomson parabola (TP) ion spectrometer. Two time-resolved diagnostics, streaked optical pyrometry (SOP) and Fourier domain interferometry (FDI), were employed to simultaneously probe the target rear surface for time history of temperature, reflectivity, and phase shift. The main target consisting of Au and C layers is located 50 μm away from the proton-generating Cu foil. Both the 100-nm Au and 78 or 150 nm

*ping2@llnl.gov

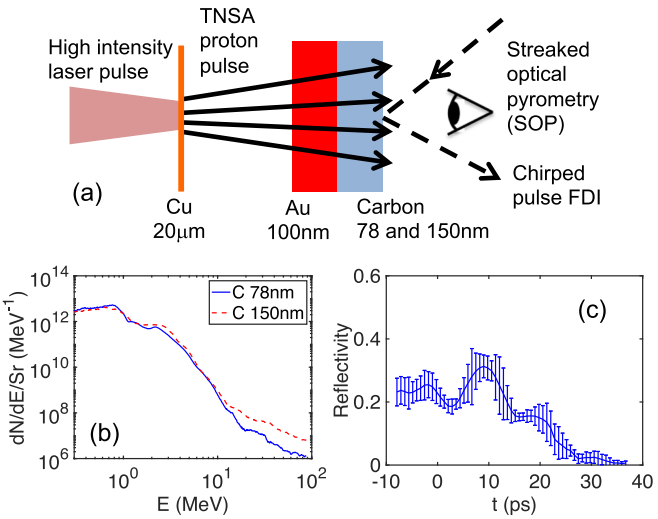

FIG. 1. (a) Experimental setup for proton heating of multilayer targets. Both the incident angle of the FDI beam and the SOP collection lens position are 16° from target normal. The temporal resolution is 6 ps in SOP and 1 ps in FDI. (b) Proton energy spectra measured by the Thomson parabola spectrometer. (c) Measured carbon reflectivity vs time.

of amorphous carbon were deposited on a 100-nm Si_3N_4 substrate to ensure an optical-quality surface for FDI measurements. The mass density of the carbon layer was measured to be 2.4 ± 0.1 g/cc. The C thickness is chosen to be optically thick for pyrometric measurements yet still thin enough so that the heat flow from the hotter Au layer can traverse the C layer and be detected before hydrodynamic cooling becomes dominant.

The proton energy spectra from the two shots for 78-nm and 150-nm carbon layers are shown in Fig. 1(b). The two spectra are very similar from the heating point of view because the heating is dominated by low-energy protons. The time-resolved reflectivity from FDI is shown in Fig. 1(c), which was used to determine the emissivity for gray-body temperature correction. The modulations near $t = 0$ in reflectivity could be caused by interference with the optical transition radiation [26] or dielectric function changes induced by the transition from the metal to vapor to plasma. The thermal conduction heat flow is diagnosed as a time-resolved thermal emission at the heated carbon rear surface by a streaked optical pyrometer (SOP) at 400 nm with 70-nm bandwidth. The finite emissivity correction is only modestly important at early time up to ∼15 ps. After that, the reflectivity is below 10% so that the system behaves like a blackbody. The error bar is assessed to be ± 15% at 0–15 ps and ±10% at later time. The velocity of the carbon surface is obtained by a time derivative of the measured phase shift. Because a phase shift can be caused by either motion or change in the refractive index, this velocity is termed an effective velocity, $v_{\rm eff}$. Since the phase shift is the relative difference before and after heating, the systematic error in the FDI measurements is canceled. Therefore, the uncertainty in the velocity is mainly statistical error, $\sim \pm 5\%$ and $\pm 8\%$ in the measurements of 78 nm and 150 nm, respectively.

III. HYDRODYNAMIC SIMULATIONS

Due to the competing processes of heat flow from thermal conduction and cooling from surface expansion, the time history of the temperature and the velocity depends on both the EOS and κ_t of carbon. To understand their effects, we have carried out hydrodynamic simulations in a 1D Cartesian geometry with HYDRA [28], a multiphysics, multidimensional, arbitrary Lagrangian-Eulerian, radiation-hydrodynamics code. The 1D geometry is valid here because the heated area diameter, which is ∼300 μm, is about 1000 times of the target thickness, which is $\leqslant$350 nm.

The on-shot proton energy spectrum from the Thomson parabola was used as the heating source since the stopping by the ultrathin multilayer target is negligible compared to the MeV proton energies. The 50-μm vacuum gap between the proton-generating foil and the main multilayer target resulted in a heating duration of ∼8 ps due to the energy-dependent time-of-flight. The proton energy deposition package has been validated in our earlier work on Au and Al. There is no *ad hoc* fitting parameter in the simulations. The numerical resolution is ∼0.3 nm. The convergence is confirmed by that doubling the number of cells resulted in less than 3% difference in the observables. Similar to our previous work on Al [24], radiation transport was included in the simulations using multigroup, implicit Monte Carlo (IMC) photonics [29] with opacity tables generated by Livermore's online opacity server. To directly compare with the SOP data, emission near 400 nm from the target was calculated and spectrally resolved using the emissivity and opacity tables in the HYDRA simulations. The effective temperature, $T_{\rm eff}$, is ∼10%–20% lower than the temperature at the critical density and in better agreement with data. The sensitivity of our observables to many hydrodynamic processes is investigated by systematically varying the corresponding properties in HYDRA simulations. It is confirmed that properties of the Si_3N_4 layer, the electron-ion equilibration rates in Au/carbon, a 1-nm-thick contamination layer of CH or H_2O at the carbon surface, and the thermal conductivity of Au have a very small effect on the observables after 15 ps. It has been identified that the properties that play a major role in the measurements are the EOS and carbon κ_t under our experimental conditions.

The evolution of the mass density and the electron temperature is displayed in Fig. 2. Two EOS tables, LEOS [30] L9061 and Sesame [31] S7833, are compared in Figs. 2(a) and 2(b) using the same κ_t model Lee-More [32]. L9061 predicts a slightly faster expansion in the density profile and slightly higher temperature after 10 ps. Figures 2(c) and 2(d) show the profiles of density and electron temperature for two κ_t models, Lee-More and GMS6 [33], while keeping the same EOS L9061. The GMS6 model predicts a much higher thermal conductivity of carbon than the Lee-More model [see Fig. 5(b) and 5(c) below], hence a higher temperature after 10 ps as seen in Fig. 2(d), and the expansion also occurs faster as seen in Fig. 2(c). It is clear that both the EOS and κ_t affect the time history of the two experimental observables. It is also noted that the differences in the EOS and κ_t models become manifest in the observables after 10 ps. This is because both the EOS and thermal conductivity are hydrodynamic quantities so that their effects become dominant only after expansion and thermal conduction have occurred.

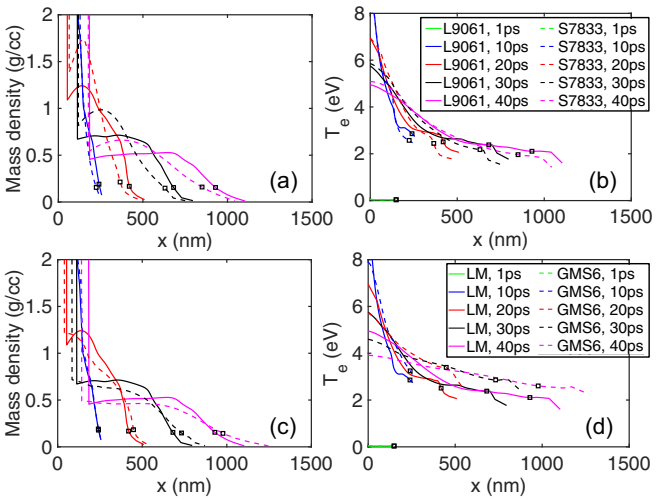

FIG. 2. HYDRA simulation results to show effects of the EOS and κ_t. (a) and (b) Density and electron temperature profiles of the carbon layer at five delays for two EOS tables, L9061 and Sesame 7833, with the same κ_t model Lee-More. (c) and (d) Similar profiles for two κ_t models, Lee-More and GMS6, with the same EOS L9061. The location of the critical density is marked by black squares.

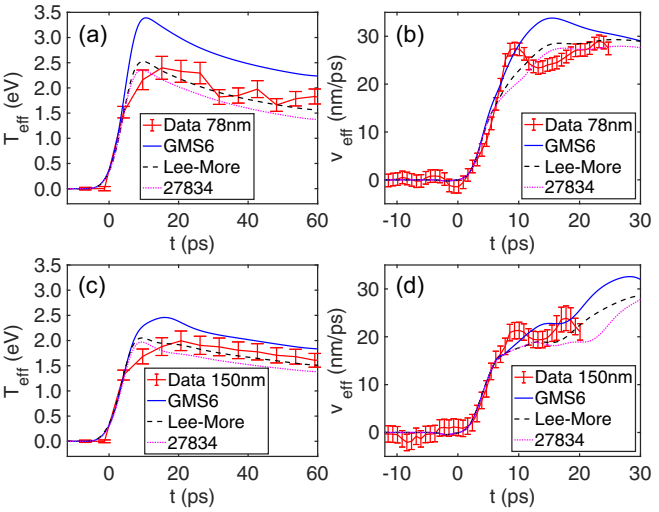

FIG. 4. Comparison of data and HYDRA simulation outputs using L9061 with three conductivity models: GMS6, Lee-More and Sesame 27834. (a) and (c) The time history of the temperature obtained from SOP. (b) and (d) The velocity obtained from FDI measurements.

IV. COMPARISON BETWEEN DATA AND SIMULATIONS

Figure 3 shows the measured temperature T_{eff} and velocity v_{eff} as a function of time for the two carbon thicknesses, together with simulations using LEOS L9061, L60, and Sesame S7833 for carbon EOSs. A timing fiducial for cross-timing the two diagnostics would be useful, yet it was impracticable because the two measurements employed very different mechanisms for time resolution. The time axis in the experimental data was adjusted to match the onset in the simulated data to ensure the relative timing between the two diagnostics is correct.

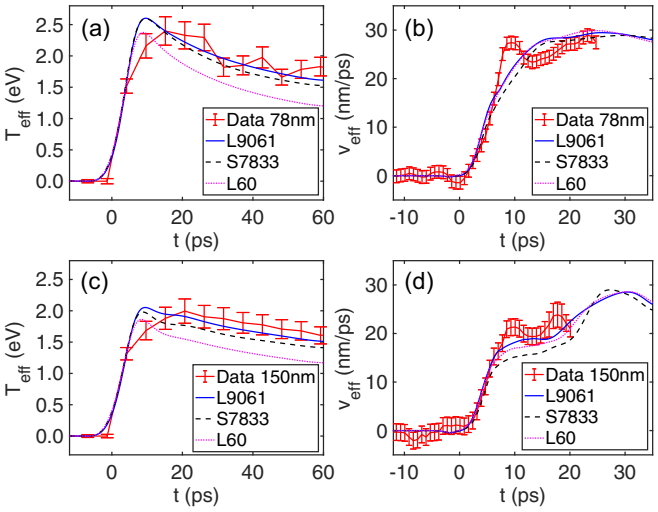

FIG. 3. Comparison of data and HYDRA simulation outputs for two carbon thicknesses. (a) and (c) The time history of the temperature obtained from SOP. (b) and (d) The velocity obtained from FDI measurements. Three EOS tables, L9061 (blue), S7833 (black), L65 (green), and Lee-More thermal conductivity are used in these simulations.

Early time discrepancy is observed in both SOP and FDI data for carbon, 78 nm and 150 nm, similar to the case of Al in our previous study, which could be due to nonequilibrium processes and phase transition effects that are not properly modeled in hydrodynamic simulations. Since expansion and thermal conduction are hydrodynamic processes occurring at a much longer timescale than the heating, EOSs and thermal conductivity models can still be tested based on late-time behaviors, which is confirmed by varying EOS thermal conductivity in the HYDRA simulations as shown in Fig. 2. In addition, both EOSs and thermal conductivity are defined under equilibrium conditions, i.e., there is a well-defined temperature. Therefore, we chose to compare the data and the simulation results at $t > 15$ ps to constrain the EOS and κ_t.

For the time history of the temperature, L9061 results agree with both 78 nm and 150 nm data after 15 ps; S7833 results are inside the error bars of the 78 nm data but slightly too low comparing to the 150 nm data; and L60 predictions are clearly too low for both thicknesses. For the comparison of measured and simulated velocities, all three EOS tables predict similar velocities in the case of 78 nm, which match the data from 15 ps up to 25 ps (end of the measurement). In the case of 150 nm, L9061 and L60 predictions are near the lower limit of the data, and S7833 results are clearly too low.

The dependence on the thermal conductivity is shown in Fig. 4. Three models that represent the low, medium, and high range of calculated κ_t, Sesame 27834, Lee-More, and GMS6, which have been implemented in HYDRA, are compared. The constant γ for the onset of melting in the Lee-More model is 1.35 in HYDRA [34] for these calculations. There are other versions of Lee-More models in the literature, including an improved version at low densities [35]. In the original Lee-More model, $\log \Lambda$ is greater than or equal to 2.0, $\log \Lambda \geqslant 2$. The GMS6 model, listed in Ref. [33] as the best

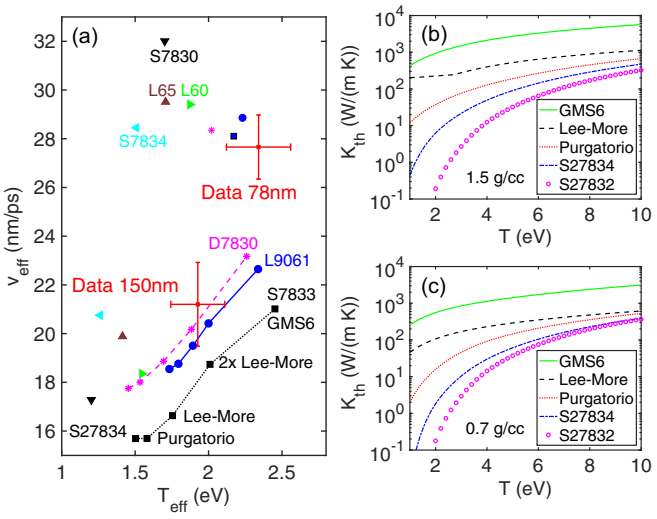

FIG. 5. (a) Velocity vs temperature near 20 ps. Two data points (78-nm- and 150-nm-thick carbon) and seven EOS tables are plotted for comparison. The effect of thermal conduction is shown as lines for the 150-nm case for three EOS tables that are closest to the data, L9061, S7833, and D7830. The five points along the line represent κ_t models S27834, Purgatorio, Lee-More, 2× Lee-More, and GMS6, respectively. (b) Thermal conductivity vs temperature predicted by five models at 1.5 g/cc. (c) Calculated thermal conductivity at 0.7 g/cc.

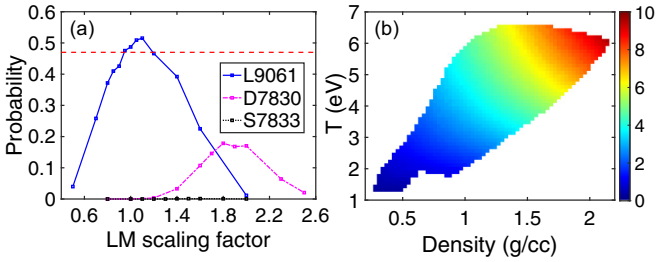

FIG. 6. (a) Probabilities of the model matching the data calculated using the χ^2 analysis with 40 points. The P_{thres} is marked as the red dashed line. (b) Thermal conductivity of carbon by 1.05× Lee-More in unit of 100 W/(m K) as a function of density and temperature. Thermal conductivities in the range of $1.05 \pm 0.15\times$ Lee-More are in agreement with the data within the experimental errors.

approximation, allows $\log \Lambda$ to go as low as 0.001. For the time history of the temperature shown in Figs. 4(a) and 4(c), the GMS6 prediction is too high compared to the SOP data, the Sesame 27834 prediction is too low, and the Lee-More prediction is within the experimental error bars after 15 ps. In the case of the velocity shown in Figs. 4(b) and 4(d), the discrepancy between the simulations and the data is larger, yet the trend stays the same.

To visualize the data-simulation comparison with more EOS and κ_t models, we choose the temperature and velocity around 20 ps to make a plot of velocity versus temperature, shown in Fig. 5(a). The time delay of 20 ps is chosen because both the temperature and the velocity are near a plateau, and it is after the initial nonequilibrium 15 ps as well as just before the end of the velocity data. The two data points in Fig. 5(a) are averaged over three points in the temperature history at 20 ± 6 ps and 10 points in the velocity history up to the end of the measurements. Seven EOS tables are included in Fig. 5(a) to compare with data: S7830, L65, L60, S7834, L9061, D7830 (developed by Sandia National Laboratories), and S7833. The first four EOSs, labeled as triangles, are very far away from the data and unlikely to match the data no matter how the thermal conductivity is changed. The last three EOSs, L9061, D7830, and S7833, are close to both data points and thus further investigated by varying thermal conductivity.

The effect of thermal conduction is presented as the dashed lines in Fig. 5(a) for L9061, S7833, and D7830 in the case of 150 nm. Five models of carbon κ_t are available for comparison: S27832, S27834, Purgatorio [8], Lee-More [32], and GMS6. Their predictions of carbon κ_t versus temperature at 1.5 g/cc are plotted in Fig. 5(b). At 3 eV the calculated κ_t varies by more than two orders of magnitude, from the lowest 3 W/(m K) in S27832 to the highest 1500 W/(m K) in the GMS6 model. We found that the thermal conductivity in S27832 is too low to show any effect in the plot of velocity versus temperature, thus it is not included in Fig. 5(a). The five points along each line represent S27834, Purgatorio, Lee-More, 2× Lee-More, and GMS6, respectively. It can be seen that high thermal conductivity increases both the temperature and velocity. S27834 and Purgatorio predictions are too low in comparison to the data. The GMS6 model overestimates κ_t and results in too high velocity and temperature in comparison to the data. The best fit to both data by varying κ_t is approximately 1×, 1.5×, and 2× Lee-More for L9061, S7833, and D7830, respectively.

The detailed data-simulation comparison on the time history of the temperature and the velocity is quantified by a statistical χ^2 analysis. Total 40 data points are used for this analysis, with 10 points from each temperature measurement at 20–80 ps and 10 points from each velocity measurement up to the end of the probing window. The χ^2 statistic, a measure of the goodness-of-fit of the model to the data, is calculated as $\chi^2 = \sum_{i=1}^{N} (\frac{x_i - s_i}{\sigma_i})^2$, where $N = 40$ is the number of points, x_i is the measured quantity, s_i the simulated quantity, and σ_i is the measurement uncertainty. The probability of a model matching the data is $P(\chi^2, N) = [1/2^{N/2}/\Gamma(N/2)] \int_{\chi^2}^{\infty} y^{N/2-1} e^{-y/2}\, dy$, where $\Gamma(z) = \int_0^{\infty} y^{z-1} e^{-y}\, dy$.

The calculated probabilities are shown in Fig. 6(a) for the three EOS tables that are closest to the data. The thermal conductivity is varied by a scaling factor in the Lee-More model since the other four κ_t models predict either too low or too high thermal conductivity as shown in Fig. 5(a). The L9061 with 1.1× Lee-More produces the highest probability, 52%. The second highest is D7830 with ∼2× Lee-More, 18%. The S7833 with any κ_t has a probability less than 2%. The probabilities of all other EOS-κ_t combinations are well below 1%. The threshold probability, defined as all the simulated quantities that are at the limits of the experimental uncertainties, i.e., $(x_i - s_i)^2 = \sigma_i^2$, $\chi^2 = N$, and $P_{\text{thres}} = P(40, 40) = 47\%$, is marked as the red dashed line in Fig. 6(a). If the probability is less than P_{thres}, the simulated quantities are on the average outside the experimental errors. It is clear from Fig. 6(a) that there is only one combination of EOS and κ_t

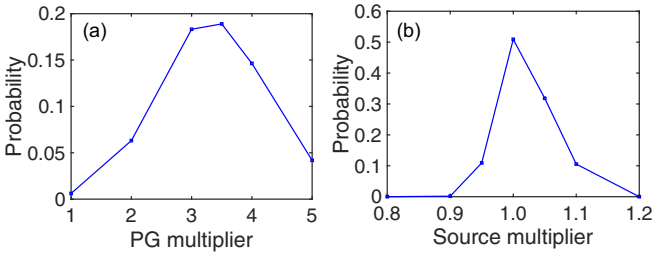

FIG. 7. (a) Probabilities of L9061 with the Purgatorio conductivity model vs the scaling factor of the Purgatorio κ_t. (b) Probabilities of L9061 with 1.05× Lee-More κ_t as a function of the proton source multiplier.

models that provides a probability above P_{thres}: L9061 and ∼1.1× Lee-More. By scanning the scaling factor of Lee-More model, thermal conductivities in the range of 1.05 ±0.15× Lee-More are in agreement with the data within the experimental errors. The thermal conductivity of carbon calculated with 1.05× Lee-More is plotted in Fig. 6(b) as a function of density and temperature, with an uncertainty of ±15% as constrained by the χ^2 analysis. Only the colored density and temperature region has been reached in the experiment presented here. The blank regions are unexplored under our experimental conditions.

V. DISCUSSION

Overall, we find that the Lee-More model multiplied by 1.05 and coupled with the L9061 EOS model provides the best agreement with the data. Sesame 7833 is a model that was built specifically for pressed powder graphite. It uses the Thomas-Fermi-Dirac model for the electron thermal component and was generated using models commonly used in Sesame database [31]. It has been parametrized to fit data reported in Ref. [36]. D7830 is a multiphase model which uses the Thomas-Fermi-Dirac model for the electron thermal term [37]. L60 is a standard QEOS-based model for carbon which also uses the Thomas-Fermi model for the electron thermal component [30]. L9061 is a Purgatorio-based EOS model that is was calibrated to match multiphase quantum simulations by Benedict *et al.* [38], thus it is considered to be one of the best available models for carbon in the regime explored in this experiment.

We also find that, in the regime explored by the experiment as shown in Fig. 6(b), the Lee-More model in the HYDRA calculations is generally a factor of three to four times larger than the values in the Purgatorio-based model. We therefore performed a second sensitivity study using the L9061 EOS model and the Purgatorio model with factors of two to five applied uniformly to the model. We find that applying a multiplier does improve the agreement of the Purgatorio model with the data as shown in Fig. 7(a), but the overall χ^2 probability is still less than 20%. In contrast to the Lee-More model which assumes specific cutoff criteria in order to solve the nonconvergent Coulomb scattering problem, the Purgatorio model is based on computing the scattering function for the electron-ion interaction based on the self-consistent scattering potential within the Ziman formulation [8,39]. The method thus incorporates a more fundamental, quantum mechanical scattering calculation than the Lee-More model and should be more accurate in the warm dense matter regime. The potential weaknesses of Purgatorio are that (1) it is an average-atom method, though the correlations between ions are incorporated via an assumed form of the ion structure factor, $S(k)$; (2) the electron-electron collisions must be incorporated via an assumed form at high temperatures, when the electrons are no longer purely degenerate; and (3) the effective number of scattering electrons is chosen based on a choice of the free electron density. The $S(k)$ approximation and the choice of the free electron density are the dominant sources of uncertainty in the warm dense matter regime. In Ref. [40] it was demonstrated that variations in $S(k)$ can easily result in differences of two to five times in the thermal conductivity. While the Lee-More model likely lacks the correct physics in the regime of these experiments, we suspect that it is compensating for some inadequacy in the structure factor used in the Purgatorio model. Other possibilities include internal cancellation of errors, such as too large conductivity in some of theρ-T space and too small elsewhere or a cancellation of errors between the EOS and κ_t models because they are not internally consistent. This is an interesting experimental result that should elicit further investigation.

The inferences made here are likely sensitive to the heating source, which is calculated with the proton energy deposition package in HYDRA and validated with the Au/Al data presented in our earlier work [24]. We also checked the results in this paper by studying how the agreement of the HYDRA calculation is affected by applying a multiplier to the energy deposition source. The probabilities of this sensitivity study are shown in Fig. 7(b). Even a 5% increase or decrease in the source would decrease the probability to below P_{thres}. This is mainly because the simulated velocity is near the upper limit of the data for 78-nm carbon, and near the lower limit of the data for 150-nm carbon as shown in Fig. 2. Changing in either way will decrease the probability of matching the data. The fact that the probability is highest at the same source multiplier as that was determined independently by Au-only data in Ref. [24] confirms the consistency with our previous study. A similar sensitivity study was performed for L9061 with the Purgatorio thermal conductivity model. We conclude that applying a modest source multiplier of less than 15% improves the agreement of the calculations using the Purgatorio thermal conductivity model and the L9061 EOS model with the data. However, the calculations that used the Lee-More model still appear to provide better agreement with the data.

As described above and in Ref. [24], discrepancy between the data and the simulations still exists at early time, likely due to nonequilibrium processes such as electron-ion coupling [41], non-Maxwellian velocity distributions upon heating [42], and phase transitions, including melting and vaporization that is not well modeled in hydrodynamic codes. In particular, taking into account vaporization-induced density disturbance or interference with optical transition radiation during heating might be helpful to explain the modulations in the reflectivity and the velocity. All these topics are active research areas but are beyond the scope of this paper. The diffusion at Au/C interface has been estimated using

plasma-based kinetic theory [43], which provided diffusivities comparable to recent molecular dynamics calculations [44]. This calculation has been described in some detail in Ref. [24]. Under our experimental conditions for carbon, the diffusion length of Au into C is about 15 nm at 60 ps, much less than the thickness of the carbon layer. Therefore, we do not expect interface diffusion to play a role in our measurements.

VI. CONCLUSION

To summarize, we have presented the first measurements on heat-release EOS and thermal conductivity for warm dense carbon by proton differential heating. At densities of 0.3–2.0 g/cc and temperatures of 1–7 eV, only L9061 EOS and $1.05 \pm 0.15\times$ Lee-More thermal conductivity agree with all data within the experimental errors. This platform can be extended to many other materials. The χ^2 statistical analysis provides a useful tool to quantify the comparison between data and simulations.

For future experiments, a carbon single-layer target should be added to constrain EOSs separately. Measurements of carbon-only targets will depend only on the EOS not on thermal conductivity, making it possible to decouple the two measurements. On the other hand, minimizing the target expansion during heat conduction will reduce dependence on EOSs. A tamping layer would be needed to minimize expansion and access compressed states. This layer is unlikely to stay transparent upon heating and compression to high pressures, hence x-ray diagnostics for spatially resolved temperature profiles would be necessary. Extending the FDI measurements to a later time will also be useful to extend the data set. Bayesian analysis can be applied to improve the statistical analysis with multiple variables. Further investigations of the early time discrepancy are certainly of interest in nonequilibrium WDM physics.

ACKNOWLEDGMENTS

This work was performed under the auspices of the U.S. Department of Energy by Lawrence Livermore National Laboratory under contract DE-AC52-07NA27344 with support from DOE OFES Early Career program and LLNl LDRD program. We thank the JLF team for laser operation and C. Cadwalader for target fabrication. H.D.W. acknowledges support from DOE via the PECASE. The UCSD team was supported by the University of California Office of the President Lab Fee Grant No. LFR-17-449059.

[1] R. P. Drake, *High-Energy-Density Physics* (Springer, Berlin, 2010).
[2] S. Le Pape, L. F. BerzakHopkins, L. Divol, A. Pak, E. L. Dewald, S. Bhandarkar, L. R. Bennedetti, T. Bunn, J. Biener, J. Crippen *et al.*, Phys. Rev. Lett. **120**, 245003 (2018).
[3] R. J. Hemley *et al.*, Science **276**, 1242 (1997).
[4] Y. Ping *et al.*, Phys. Rev. Lett. **111**, 065501 (2013).
[5] M. Ross, Nature (London) **292**, 435 (1981).
[6] J. H. Eggert *et al.*, Nat. Phys. **6**, 40 (2010).
[7] G. A. Rinker, Phys. Rev. B **31**, 4220 (1985); Phys. Rev. A **37**, 1284 (1988).
[8] P. Sterne, S. Hansen, B. Wilson, and W. Isaacs, High Energy Density Phys. **3**, 278 (2007).
[9] G. Faussurier, C. Blancard, P. Combis, and L. Videau, Phys. Plasmas **21**, 092706 (2014).
[10] S. Kuhlbrodt and R. Redmer, Phys. Rev. E **62**, 7191 (2000).
[11] H. D. Whitley *et al.*, Contrib. Plasma Phys. **55**, 192 (2015).
[12] F. R. Graziani *et al.*, High Energy Density Phys. **8**, 105 (2012).
[13] D. E. Hanson, L. A. Collins, J. D. Kress, and M. P. Desjarlais, Phys. Plasmas **18**, 082704 (2011).
[14] M. P. Desjarlais, C. R. Scullard, L. X. Benedict, H. D. Whitley, and R. Redmer, Phys. Rev. E **95**, 033203 (2017).
[15] S. X. Hu, L. A. Collins, T. R. Boehly, J. D. Kress, V. N. Goncharov, and S. Skupsky, Phys. Rev. E **89**, 043105 (2014); S. X. Hu *et al.*, Phys. Plasmas **23**, 042704 (2016).
[16] M. Dharma-wardana and F. Perrot, Phys. Lett. A **163**, 223 (1992).
[17] R. F. Smith *et al.*, Nature (London) **511**, 330 (2014).
[18] D. K. Bradley *et al.*, Phys. Rev. Lett. **102**, 075503 (2009).
[19] K. Falk, E. J. Gamboa, G. Kagan, D. S. Montgomery, B. Srinivasan, P. Tzeferacos, and J. F. Benage, Phys. Rev. Lett. **112**, 155003 (2014).
[20] M. C. Gregor *et al.*, Phys. Rev. B **95**, 144114 (2017).
[21] K. Falk, M. Holec, C. J. Fontes, C. L. Fryer, C. W. Greeff, H. M. Johns, D. S. Montgomery, D. W. Schmidt, and M. Šmíd, Phys. Rev. Lett. **120**, 025002 (2018).
[22] P. McKenna, A. P. L. Robinson, D. Neely, M. P. Desjarlais, D. C. Carroll, M. N. Quinn, X. H. Yuan, C. M. Brenner, M. Burza, M. Coury *et al.*, Phys. Rev. Lett. **106**, 185004 (2011).
[23] Y. Ping *et al.*, Phys. Plasmas **22**, 092701 (2015).
[24] A. McKelvey *et al.*, Sci. Rep. **7**, 7015 (2017).
[25] P. K. Patel *et al.*, Phys. Rev. Lett. **91**, 125004 (2003).
[26] G. M. Dyer *et al.*, Phys. Rev. Lett. **101**, 015002 (2008).
[27] S. Feldman, G. Dyer, D. Kuk, and T. Ditmire, Phys. Rev. E **95**, 031201(R) (2017).
[28] M. M. Marinak *et al.*, Phys. Plasmas **8**, 2275 (2001).
[29] J. A. Fleck Jr. and J. D. Cummings, J. Comput. Phys. **8**, 313 (1971).
[30] LEOS data library is based on a QEOS-like model described in R. M. More, K. H. Warren, D. A. Young, and G. B. Zimmerman, Phys. Fluids **31**, 3059 (1988); D. A. Young and E. M. Corey, J. Appl. Phys. **78**, 3748 (1995).
[31] B. Bennett, J. Johnson, G. Kerley, and G. Rood, *Recent Developments in the Sesame Equation-of-State Library* (1978); S. P. Lyon and J. D. Johnson (eds.), Sesame: The Los Alamos National Laboratory Equations of State Database, Los Alamos National Laboratory Report LA-UR-92-3407 (1992).
[32] Y. T. Lee and R. M. More, Phys. Fluids **27**, 1273 (1984).
[33] D. O. Gericke, M. S. Murillo, and M. Schlanges, Phys. Rev. E **65**, 036418 (2002).

[34] This constant originated from a private communication with R. M. More.

[35] M. P. Desjarlais, Contrib. Plasma Phys. **41**, 267 (2001); M. P. Desjarlais, J. D. Kress, and L. A. Collins, Phys. Rev. E **66**, 025401(R) (2002).

[36] R. W. Ohse and H. Tippelskirch, High Temp. High Press. **9**, 367 (1977).

[37] G. I. Kerley and L. Chhabidas, Multicomponent-multiphase equation of state for carbon, Sandia report SAND2001-2619 (2001).

[38] L. X. Benedict, K. P. Driver, S. Hamel, B. Militzer, T. Qi, A. A. Correa, A. Saul, and E. Schwegler, Phys. Rev. B **89**, 224109 (2014).

[39] R. Evans, B. L. Gyorffy, N. Szabo, and J. M. Ziman, in *The Properties of Liquid Metals*, edited by S. Takeuchi (Wiley, New York, 1973), p. 319.

[40] C. E. Starrett, High Energy Density Phys. **19**, 58 (2016).

[41] Z. Chen, B. Holst, S. E. Kirkwood, V. Sametoglu, M. Reid, Y. Y. Tsui, V. Recoules, and A. Ng, Phys. Rev. Lett. **110**, 135001 (2013).

[42] N. Medvedev, U. Zastrau, E. Forster, D. O. Gericke, and B. Rethfeld, Phys. Rev. Lett. **107**, 165003 (2011).

[43] S. Chapman and T. Cowling, *The Mathemtical Theory of Non-uniform Gases: An Account of the Kinetic Theory of Viscosity, Thermal Conduction and Diffusion in Gases* (Cambridge University Press, Cambridge, 1970).

[44] T. Haxhimali and R. E. Rudd, in *Frontiers and Challenges in Warm Dense Matter*, edited by F. Graziani, M. Desjarlais, R. Redmer and S. Trickey, Lecture Notes in Computational Science and Engineering Vol. 96 (Springer International Publishing, Cham, Switzerland, 2014).